Acta Biomaterialia 125 (2021) 219–230

Contents lists available at ScienceDirect

Acta Biomaterialia

journal homepage: www.elsevier.com/locate/actbio

Full length article

Cryptic ligand on collagen matrix unveiled by MMP13 accelerates bone tissue regeneration via MMP13/Integrin α3/RUNX2 feedback loop

Yoshie Arai[a], Bogyu Choi[b], Byoung Ju Kim[a], Sunghyun Park[b], Hyoeun Park[a], James J. Moon[c], Soo-Hong Lee[a,*]

[a] Department of Medical Biotechnology, Dongguk University-Seoul, 04620 Seoul, Republic of Korea
[b] Department of Biomedical Science, CHA University, CHA Biocomplex, 335, Pangyo-ro, Bundang-gu, Seongnam-si, Gyeonggi-do, 13488, Republic of Korea
[c] Department of Pharmaceutical Sciences, Department of Biomedical Engineering & Biointerfaces Institute, University of Michigan, Ann Arbor, MI 48109, United States

ARTICLE INFO

Article history:
Received 28 September 2020
Revised 23 February 2021
Accepted 25 February 2021
Available online 4 March 2021

Keywords:
Matrix metalloproteinases
ECM remodeling
Bond tissue regeneration
Self-healing
Mesenchymal stem cells

ABSTRACT

Extracellular matrix (ECM) remodeling is necessary for the development and self-healing of tissue, and the process is tissue specific. Matrix metalloproteinases (MMPs) play a role in ECM remodeling by unwinding and cleaving ECM. We hypothesized that ECM remodeling by MMPs is involved in the differentiation of stem cells into specific lineages during self-healing. To prove the hypothesis, we investigated which MMPs are involved in the osteogenic differentiation of human mesenchymal stem cells (hMSCs) grown on a type I collagen (Col I) matrix, and we found that specifically high expression of MMP13 in hMSCs grown on a Col I matirx during osteogenic differentiation. Moreover, knocking down of *MMP13* decreased the osteogenic differentiation of hMSCs grown on a Col I matrix. In addition, pre-treatment of recombinant human MMP13 lead to remodeling of Col I matrix and increased the osteogenic differentiation of hMSCs and in vivo bone formation following the upregulation of the expression of runt-related transcription factor 2 (RUNX2), integrin α3 (ITGA3), and focal adhesion kinase. Furthermore, the transcription factor RUNX2 bound to the *MMP13* promoter. These results suggest that growth on a remodeled Col I matrix by MMP13 stimulates osteogenic differentiation of hMSCs and self-healing of bone tissue via an MMP13/ITGA3/RUNX2 positive feedback loop.

Statement of significance

Self-healing of tissue could be the key to treating diseases that cannot be overcome by present technology. We investigated the mechanism underlying the self-healing of tissue and we found that the osteogenic differentiation was increased in hMSCs grown on a remodeled Col I matrix by the optimized concentration of MMP13 not in hMSCs grown on a Col I fragments cleaved by a high concentration of MMP13. In addition, we found the remodeled Col I matrix by MMP13 increased the osteogenic capacity through a MMP13/integrin α3/RUNX2 positive feedback loop. This result would be able to not only provide a strategy for bone tissue-specific functional materials following strong evidence about the self-healing mechanism of bone through the interaction between stem cells and the ECM matrix. As such, we strongly believe our finding will be of interest to researchers studying biomaterials, stem cell biology and matrix interaction for regenerative medicine and therapy.

1. Introduction

Stem cells home to sites of injury and stimulate self-healing [1–5]; they can also differentiate into specific cell types and indirectly induce cytokine release and modulation of the microenvironment, including the surrounding extracellular matrix (ECM). For instance, stem cells are involved in the early stages of bone fracture repair through the generation of bone cells and ECM remodeling. Differentiated cells can reinforce the fracture callus, and the remodeled ECM provides structural support for cells. A large proportion of bone tissue is composed of inorganic ECM (hydroxyap-

* Corresponding author.
E-mail address: soohong@dongguk.edu (S.-H. Lee).

https://doi.org/10.1016/j.actbio.2021.02.042
1742-7061/

atite) and organic ECM components, such as collagen, fibronectin, laminin, vitronectin, and osteopontin [6,7]. The interactions of cells with organic ECM molecules regulate their differentiation, proliferation, and survival [8,9]; therefore, ECM has been studied extensively in the fields of bone regeneration and engineering [10–12]. One of the ECM proteins, type I collagen (Col I), has a unique triple-helical structure and is known to promote osteogenic differentiation [10,13,14]. In this study, we used a Col I matrix to investigate the mechanisms underlying the self-healing of bone tissue.

Matrix metalloproteinases (MMPs), a family of zinc-dependent proteolytic enzymes, are secreted by osteoblasts and osteoclasts and mediate ECM remodeling [15]. Specifically, MMP2, MMP9, MMP13, and MMP14 play important roles in bone formation and remodeling [15,16]. MMP13, in particular, can bind to the collagen matrix and regulate collagen remodeling [17], and its expression is increased in osteoblastic cells, as MMP13 is required for the initial modeling of long bones during development [18–21]. MMP13-deficient mice show abnormal bone phenotypes, such as endochondral bone malformation [22,23], and MMP13-knock-out mice have an impaired ability to repair long bone fractures [24]. Furthermore, the promoter of the MMP13 is a target of the osteogenic markers runt-related transcription factor 2 (RUNX2) and osterix (OSX), which are osteogenic markers [19,25,26]. Lastly, MMP13 has been suggested to play an important role in the osteogenic differentiation of mesenchymal stem cells (MSCs).

During bone ECM remodeling, MMPs change the extracellular environment and regulate cell adhesion molecules such as integrins [1,8]. As a ligand (agonist), the remodeled ECM by MMPs bind to the cytoplasmic tail of a heterodimeric integrin composed of α and β subunits. This stimulates a downstream signaling cascade, including the phosphorylation of focal adhesion kinase (FAK), which regulates the fate of stem cells [27,28]. The integrins $\alpha v\beta 1$, $\alpha v\beta 3$, $\alpha 2\beta 1$, $\alpha 3\beta 1$, $\alpha 4\beta 1$, $\alpha 5\beta 1$, and $\alpha 11\beta 1$ are activated during the osteogenic differentiation of human MSCs (hMSCs) [29–34], and activated integrins induce the expression of osteogenic markers, including RUNX2 and OSX [29]. Several integrins, e.g., $\alpha 1\beta 1$, $\alpha 2\beta 1$, $\alpha 10\beta 1$, and $\alpha 11\beta 1$, bind to the triple-helical structure of Col I [35,36]. Therefore, remodeling of the ECM by certain MMPs may be associated with the expression of specific integrins; for example, Tang et al. reported that MT1-MMP increases integrin $\beta 1$ (ITGB1) activity in skeletal stem cells [37]. However, it is unclear how remodeling of the Col I matrix by MMPs influences the osteogenic differentiation of hMSCs. Herein, we hypothesized that Col I matrix remodeling by MMP13 is a pivotal event during bone self-healing in humans. We focused on the mechanisms linking the ECM and MMPs during the osteogenic differentiation of hMSCs. Our results indicated that MMP13 plays a crucial role in the osteogenic differentiation of hMSCs grown on a Col I matrix via the upregulation of integrin $\alpha 3$ (ITGA3) and, thereby, increases cell-ECM binding. In addition, a recombinant human MMP13 (rhMMP13)-treated Col I sponge significantly enhanced bone tissue regeneration in vivo, suggesting it could be employed as a bone-tissue-specific matrix.

2. Materials and methods

2.1. Cell culture

hMSCs were isolated from an infrapatellar fat pad of the patients' knee with approval of the Ethics Committee at CHA University (IRB No. BD2014–097). In brief, the infrapatellar fat pad were washed with Dulbecco's phosphate-buffered saline (DPBS) containing 2% (v/v) penicillin/streptomycin (p/s; Hyclone) and digested using Dulbecco's minimal essential medium/low glucose (DMEM/LOW; Hyclone, USA) containing 0.5 mg ml^{-1} collagenase type II (Sigma) at 37 °C for 40 min. hMSCs were cultured in growth medium [(DMEM/LOW) supplemented with 10% (v/v) fetal bovine serum (FBS; Hyclone) and 1% (v/v) p/s], maintained at 37 °C in a 5% CO_2 incubator, and passaged at 80% cell confluency. The osteogenic differentiation of hMSCs was induced with osteogenic medium [DMEM/high glucose (DMEM/HIGH) supplemented with 10% FBS, 10 mM β-glycerophosphate disodium salt hydrate (Sigma), 50 μg ml^{-1} L-ascorbic acid (Sigma), 100 nM dexamethasone (Dex; Sigma), 1 × GlutaMAX (Gibco)]. All experiments were performed in accordance with the IRB requirements. Informed consent was obtained from the human participants of this study.

2.2. Col I matrix coating of culture plates and treatment with rhMMP13

Cell culture plates were coated with Col I matrix at 50 μg ml^{-1} (Corning, cat#354,249) in DPBS and kept at 4 °C overnight. The Col I matrix was aspirated and washed with DPBS three times. To remodel the Col I matrix, 50 ng ml^{-1}, 100 ng ml^{-1}, or 200 ng ml^{-1} of activated rhMMP13 (R&D systems) was added to the Col I-coated plates at 37 °C for 2 h. The rhMMP13 was activated by 1 mM 4-aminophenylmercuric acetate (APMA) at 37 °C for 1 h before being added to the Col I-coated plates. The activated rhMMP13-treated plates were washed with DPBS three times. The DPBS was aspirated immediately before hMSC seeding for experimental analysis.

2.3. Alkaline phosphatase (ALP) activity, mineralization, and calcium deposition in hMSCs

ALP activity, mineralization, and calcium deposition in hMSCs cultured in osteogenic medium were detected by ALP staining and extraction, Alizarin Red S (ARS; Sigma) staining, and calcium assay, respectively. ALP in hMSCs was stained with BCIP-NBT substrate solution (Sigma-Aldrich) and visualized under an inverted microscope (Olympus, Japan). To quantify ALP activity, 4-nitrophenol solutions (0.025, 0.05, 0.1, 0.25, 0.5, and 1 mM; Sigma) were used as a standard. The standard samples and cells were incubated with 4-nitrophenyl phosphate disodium salt solution (pNPP; Sigma) at 37 °C for 15 min. The absorbance of pNPP, which was reacted with ALP, was measured at 405 nm using a microplate reader (Molecular Devices). To investigate ARS staining, ARS extraction, and the calcium assay, cells were fixed with 4% paraformaldehyde solution (Biosesang, Korea) at room temperature (RT) for 10 min and washed with distilled water. Then, 2% (w/v) ARS solution (pH 4.1–4.3) was added to the fixed cells, which were incubated at RT in the dark for 30 min. ARS solution was removed, and the cells were washed three times with distilled water. The ARS stain was extracted by 10% (v/v) cetylpyridinium chloride (dissolved in distilled water), and the absorbance was measured at 562 nm. Calcium deposition in hMSCs was detected using QuantiChrom calcium assay kit (BioAssay Systems, USA).

2.4. Quantitative RT-PCR analysis

Total RNA was isolated from hMSCs grown on a Col I matrix or uncoated plates using TRIzol reagent (Invitrogen). The extracted mRNA was converted into cDNA using the Takara cDNA synthesis kit (Takara, Japan). The gene-specific primers designed to amplify the target genes are provided in Table S1. All amplifications were performed in a final reaction mixture (50 μl) containing 25 μl of Power SYBR Green PCR Master Mix (Applied Biosystems), 0.5 μl of gene-specific primers (5 μM), 5 μl of template, and 19 μl of deionized water using a StepOnePlus Real-Time PCR system (Applied Biosystems) with the following conditions: an initial denatu-

ration at 95 °C for 1 min, followed by 45 cycles of 95 °C for 15 s, 56 °C for 15 s, and 72 °C for 15 s, and a final extension at 72 °C for 5 min. Ribosomal protein S18 (*RPS18*) and hydroxymethylbilane synthase (*HMBS*) were used for normalization of qPCR data.

2.5. Western blot analysis

hMSCs were washed three times with DPBS, and cells were lysed with 200 μl RIPA buffer (Sigma-Aldrich). Cell extracts were collected in 1.5-ml tubes and centrifuged at 13,000 rpm for 20 min. The concentration of total protein was determined using Pierce BCA protein assay kit (Thermo Scientific). The cell total protein was loaded onto a sodium dodecyl sulfate-polyacrylamide gel and separated during gel electrophoresis. The loaded proteins were transferred to a polyvinylidene fluoride membrane (PVDF; Bio-Rad, Hong Kong) with Tris-glycine-SDS-methanol transfer buffer. The membrane was blocked with 5% (w/v) skimmed milk (BD) in Tris-buffered saline containing 0.1% (v/v) Tween-20 (TBS-T; DYNE BIO, Korea) and incubated with appropriate primary antibody in 5% (w/v) bovine serum albumin (BSA) with TBS-T at 4 °C overnight to allow the primary antibody to bind specifically to the target protein. The blot was washed three times with TBS-T and incubated with a horseradish peroxidase-conjugated secondary antibody in 5% skimmed milk in TBS-T. The band for the target protein was detected with enhanced chemiluminescence (GE Healthcare Life Sciences) by ChemiDoc XRS+ system (Bio-Rad). Images of uncropped western blots are shown in Fig. S14. Details of the antibodies used are provided in Table S2.

2.6. Immunofluorescence staining

hMSCs were seeded at 100 cells per cm^2 on a 12-mm Ø coverslip (Marienfeld-Superior) either coated or not coated with Col I matrix and incubated for 24 h. Cells were washed with DPBS and fixed with 4% paraformaldehyde at RT for 10 min. Fixed cells were washed with DPBS and permeabilized in 0.03% (v/v) Triton X-100 in DPBS (PBS-T) at RT for 10 min and then blocked with 1% (w/v) BSA in DPBS at RT for 1 h. The primary antibody was diluted 1:200 in PBS-T with 1% BSA, incubated at RT for overnight, and washed with DPBS three times. Then, the cells were blocked with 1% BSA in DPBS at RT for 1 h. Fluorescein-conjugated secondary antibodies and phalloidin (Texas Red Phalloidin; Invitrogen) were diluted 1:200 in PBS-T with 1% BSA and allowed to stain the cells at RT for 1 h. The cells were washed three times with DPBS. Cellular DNA was counterstained with 0.2 μg ml^{-1} of 4′, 6-diamidino-2-phenylindole (DAPI; Invitrogen) in DPBS. The details of the antibodies are provided in Table S3.

2.7. Measurement of MMP13 using fluorescence resonance energy transfer (FRET) peptide

To explore the MMP13 activity in hMSCs grown on a Col I matrix during osteogenic differentiation, we used an MMP13-specific FRET peptide (SensoLyte Plus 520 MMP13 assay kit, AnaSpec, Inc., USA). When the FRET peptide was cleaved by MMP13, fluorescence appeared and was detectable with a fluorescence reader. Activated MMP13 was measured according to the manufacturer's protocol. Fresh medium was added 24 h before media collection. The medium containing MMP13 was collected on days 1, 3, 7, and 14 and added to anti-MMP13-antibody-coated plates, which were incubated at RT for 2 h. The plate was washed four times with 1 × wash buffer and incubated with 1 mM 4-aminophenylmercuric acetate at 37 °C for 40 min, then MMP13 substrates were added and incubated at 37 °C for 60 min. The fluorescence intensity was measured at excitation/emission wavelengths of 490/520 nm by Cytation 3 cell imaging multi-mode reader (BioTek).

2.8. Coating cell culture plates with various matrices

To compare *MMP13* expression in hMSCs grown on various matrices [Col I, gelatin, type II collagen (Col II), fibronectin (FN), and laminin(LN)], 100 μg ml^{-1} of type I collagen (Corning, cat#354,249), 1 mg ml^{-1} of gelatin (Sigma, cat#G1890), 100 μg ml^{-1} of Col II (Sigma, cat#C9301), 50 μg ml^{-1} of FN (Sigma, cat#F2006), and 100 μg ml^{-1} of LN (Sigma, cat#L2020) were dissolved in DPBS and used to coat cell culture plates by incubating at 4 °C overnight.

2.9. RNA interference

For RNA interference, we used siRNA of *MMP13* (siMMP13; Qiagen) and siRNA of *ITGA3* (siITGA3; Bioneer, Korea). The siRNA sequences targeted the sense strand of *MMP13* (5′-AACGAAATATCAAAGTCATTA-3′) and *ITGA3* (5′-GACAGUGAUGGGUGAGUCU-3′). A control siRNA (siControl; Dharmacon) was used as a control. hMSCs were seeded on 6-well plates at a density of 2 × 10^4 cells per cm^2. Then, 24 h after incubation, 20 nM of siRNA was transfected into hMSCs by Lipofectamine RNAiMAX (Invitrogen) at 37 °C for 6 h. The siRNA-treated cells were recovered for 48 h in fresh growth medium.

2.10. FITC-labeling of integrin $\alpha 3\beta 1$ (ITGA3B1)

To investigate binding of ITGA3B1 and rhMMP13-treated Col I, fluorescein isothiocyanate isomer I (FITC; Sigma) was conjugated to ITGA3B1 (R&D systems, cat#2840-A3–050). BSA was used as a control. ITGA3B1, BSA, and FITC were dissolved at 1 mg ml^{-1} in binding buffer (0.1 M carbonate-bicarbonate buffer, pH 9.0). FITC solution (10 µl) was added to 990 µl of ITGA3B1 or BSA diluent solution, and the mixture was incubated at RT in the dark for 2 h. The mixture was filtered to a 10 kDa molecular weight cut-off (Amicon Ultra centrifugal filter units; Sigma-Aldrich) and washed with DPBS to remove excess FITC. The FITC conjugation of ITGA3B1 or BSA was confirmed by the measurement of protein and the fluorescence intensity based on the BSA and FITC standards, respectively. The Col I matrix was treated with 50 ng ml^{-1} of activated rhMMP13 at 37 °C for 2 h, and 50 µl of FITC-conjugated ITGA3B1 (ITGA3B1-FITC) or BSA (BSA-FITC) was added to a non-treated Col I matrix or activated rhMMP13-treated Col I matrix and incubated at 37 °C for 1 h. The binding of ITGA3B1-FITC and the rhMMP13-treated Col I was visualized using a Cytation 3 cell imaging multi-mode reader (BioTek).

2.11. Detection of unwound Col I matrix using 5-FAM-conjugated collagen hybridizing peptide

To unwind the triple-helical structure of the Col I matrix, 50 ng ml^{-1} of activated rhMMP13 was added to Col I-coated plates with 50 μg ml^{-1} Col I matrix and incubated at 37 °C for 2 h. The rhMMP13-treated Col I matrix was incubated with 20 µM of 5-FAM-conjugated collagen hybridizing peptide (F-CHP) in PBS at 4 °C for 2 h and washed three times with PBS for 5 min. Then, a stained rhMMP13-treated Col I matrix was visualized, and we quantified the fluorescence intensity using the Cytation 3 cell imaging multi-mode reader (BioTek).

2.12. In vivo experiment using bone defect model in rat or mouse

In this study, we investigated using three types of animal models (a rat diaphysis defect model, a rat epiphysis defect model, and a mouse calvarial defect model) to confirm the bone regenerative

effect of rhMMP13-treated Col I sponge. The Col I sponge (CollaCote, Integra Life Sciences Co., USA) was adjusted to the appropriate dimension (5 × 5 mm, 1 mm in thickness), and 1 mg Col I sponge was treated with 1 μg rhMMP13 (R&D systems) for 2 h at 37 °C. DPBS-treated Col I sponge was used as a control. After rhMMP13 treatment, the sponges were washed with DPBS three times. A diaphysis or epiphysis defect model was fabricated using 8-week-old rats (Orientbio, Korea). Defects of 2 mm in diameter were generated on the long bones using a twist drill bit (Jeung Do Bio & Plant Co., Ltd., Korea) and the Col I sponge or rhMMP13-treated Col I sponge was implanted into defective site using forceps. Four weeks after implantation, the rat long bones were harvested and fixed with 4% paraformaldehyde solution. Bone formation in six rats with diaphysis or epiphysis defects was analyzed by micro-computed tomography (micro-CT) and histological staining. A calvarial defect model was fabricated using 6-week old mice (Orientbio, Korea) and Critical-sized calvarial defects 4 mm in diameter were generated on the cranium by trephine bur 3.8 (Dentech Corporation, Japan) and the Col I sponge or rhMMP13-treated Col I sponge was implanted into defective site. Eight weeks after implantation, the mouse calvaria was harvested and fixed with 4% paraformaldehyde solution. Bone formation in the calvaria defect of five mice was analyzed by micro-CT and histological staining. All animal experiments were approved by the Institutional Animal Care and Use Committee of CHA University (IACUC180063), and experiments were performed in accordance with all relevant ethical regulations and used approved study protocols. For the histological staining, the fixed tissues were treated with decalcification solution (RapidCal Immuno; BBC Biochemical, USA), dehydrated with ethanol and xylene, and embedded in paraffin. The paraffinized specimens were sliced into 4-μm sections using a semi-motorized rotary microtome (Leica, RM2245). The sections were de-paraffinized with xylene and ethanol and washed with DPBS, then stained using hematoxylin and eosin or Masson's trichrome staining solution. The stained sections were washed with DPBS three times and visualized using an inverted microscope (Olympus, Japan).

2.13. Statistical analysis

For the in vivo studies, we used a sample size of five per group based on our published studies using a preclinical rat model. We used male animals to exclude variability from the influence of female hormones in bone tissue regeneration. In addition, the details of experimental groups were blinded to the investigators for the biochemical and histological evaluations. All statistics were performed with Prism ver. 8 (GraphPad software). The one-way ANOVA test using Tukey-Kramer *post hoc* test, two-way ANOVA test using Bonferroni *post hoc* test, and unpaired *t*-test were performed. Data were considered statistically significant for $P < 0.05$. The exact *P*-values for each figure can be found in Table S4.

3. Results

3.1. Growth on a Col I matrix induces osteogenic differentiation of hMSCs via activation of focal adhesion proteins and nuclear translocation of RUNX2

Col I matrix, as a major component of the bone ECM, showed high expression levels in bone defect regions and promoted the osteogenic differentiation of hMSCs (Fig. S1 and S2). The adhesion of hMSCs grown on the Col I matrix was greater than that of hMSCs grown on uncoated plates (Fig. S2A). In addition, the proliferation of hMSCs grown on the Col I matrix was greater than that of hMSCs grown on uncoated plates after 14 days of osteogenic differentiation (Fig. S2B). However, cell morphology did not differ between these two groups of hMSCs (Fig. S2C). The ALP concentration, intensity of ARS staining, and calcium content were 1.2-, 3-, and 1.8-fold higher (respectively) in hMSCs cultured on the Col I matrix than those cultured on uncoated plates after 14 days of osteogenic differentiation (Fig. S2D–F). The mRNA expression of osteogenic marker genes [*ALP, osteopontin (OPN), bone sialoprotein (BSP), osteocalcin (OCN), RUNX2*, and *type I collagen* (*COL1)]* was significantly increased 1.5 to 38-fold in hMSCs grown on a Col I matrix after 14 days of osteogenic differentiation (Fig. S2G). RUNX2 and BSP protein levels were consistently increased in hMSCs grown on a Col I matrix, and the mRNA expression of *ITGB1* and *Vinculin* (Fig. S2H) and protein expression of vinculin (green; Fig. S2I, upper panel) and phospho-FAK (Y397) (green; Fig. S2I, lower panel), an active form of FAK, were much higher in IF images of hMSCs grown on a Col I matrix than in those on uncoated plates. The western blot analysis of vinculin and phospho-FAK (Y397) was consistent with the IF data (Fig. S2J). Expression of the active form of AKT (phospho-AKT [S473]) also increased in cells grown on the Col I matrix. RUNX2 was largely located inside the nucleus of hMSCs grown on the Col I matrix, demonstrating that it translocated from the cytosol to the nucleus (Fig. S2K, L). In summary, hMSC culture on the Col I matrix induced the activation of focal adhesion molecules and nuclear translocation of RUNX2 without altering cell morphology. These results indicate that growth on a Col I matrix promotes the osteogenic differentiation of hMSCs.

3.2. Growth on a Col I matrix and inflammatory conditions promote MMP13 expression in hMSCs

To determine which MMP family members are involved in ECM remodeling during the osteogenic differentiation of hMSCs grown on a Col I matrix, we investigated the expression of MMP genes (*MMP1, MMP2, MMP3, MMP8, MMP9, MMP10, MMP11, MMP12, MMP13, MMP14*, and *MMP19*) in hMSCs after 3 days of osteogenic differentiation (Fig. 1A). Col I matrix culture conditions decreased *MMP2* (gelatinase A) expression but significantly increased the expression of *MMP1* (collagenase-1) and *MMP13* (collagenase-3). The mRNA expression of *MMP13* increased 24 h after seeding hMSCs onto a Col I matrix but not when they were grown on uncoated plates (Fig. 1B). In addition, *MMP13* expression was increased in human bone marrow-derived MSCs (BMMSCs), which are MSCs derived from a different origin, when grown on a Col I matrix (Fig. S3). Western blot analysis demonstrated that the protein level of MMP13 in hMSCs grown on a Col I matrix was increased after 3 and 14 days of osteogenic differentiation (Fig. 1C). Secreted MMP13 was measured using an MMP13-specific cleavable FRET peptide (Fig. 1D). The level of secreted MMP13 was approximately 20 ng ml^{-1} higher for hMSCs grown on a Col I matrix than for those grown on uncoated plates after 7 and 14 days of osteogenic differentiation. However, MMP13 expression was not increased in the cells grown on other types of substrates, such as gelatin, type II collagen, fibronectin, or laminin (Fig. 1E). These data demonstrate that growth on a Col I matrix stimulates MMP13 expression during the osteogenic differentiation of stem cells.

To determine the expression of MMP13 by hMSCs during inflammation, the inflammatory inducers interleukin-1β (IL-1β), lipopolysaccharide (LPS), interferon-γ (IFN-γ), interleukin-6 (IL-6), or tumor necrosis factor-α (TNF-α) were introduced to the hMSC culture. Before treatment with the inflammatory inducers, the hMSCs were cultured in serum-free medium for 18 h with starvation. hMSCs grown on uncoated plates or Col I matrix were treated with IL-1β or LPS at 100 ng ml^{-1} for 24 h (Fig. S4A). The culture medium with IL-1β- or LPS-pre-treated hMSCs was then collected 24 h after treatment. The results demonstrated that MMP13 secretion significantly increased in IL-1β- or LPS-pre-treated hMSCs

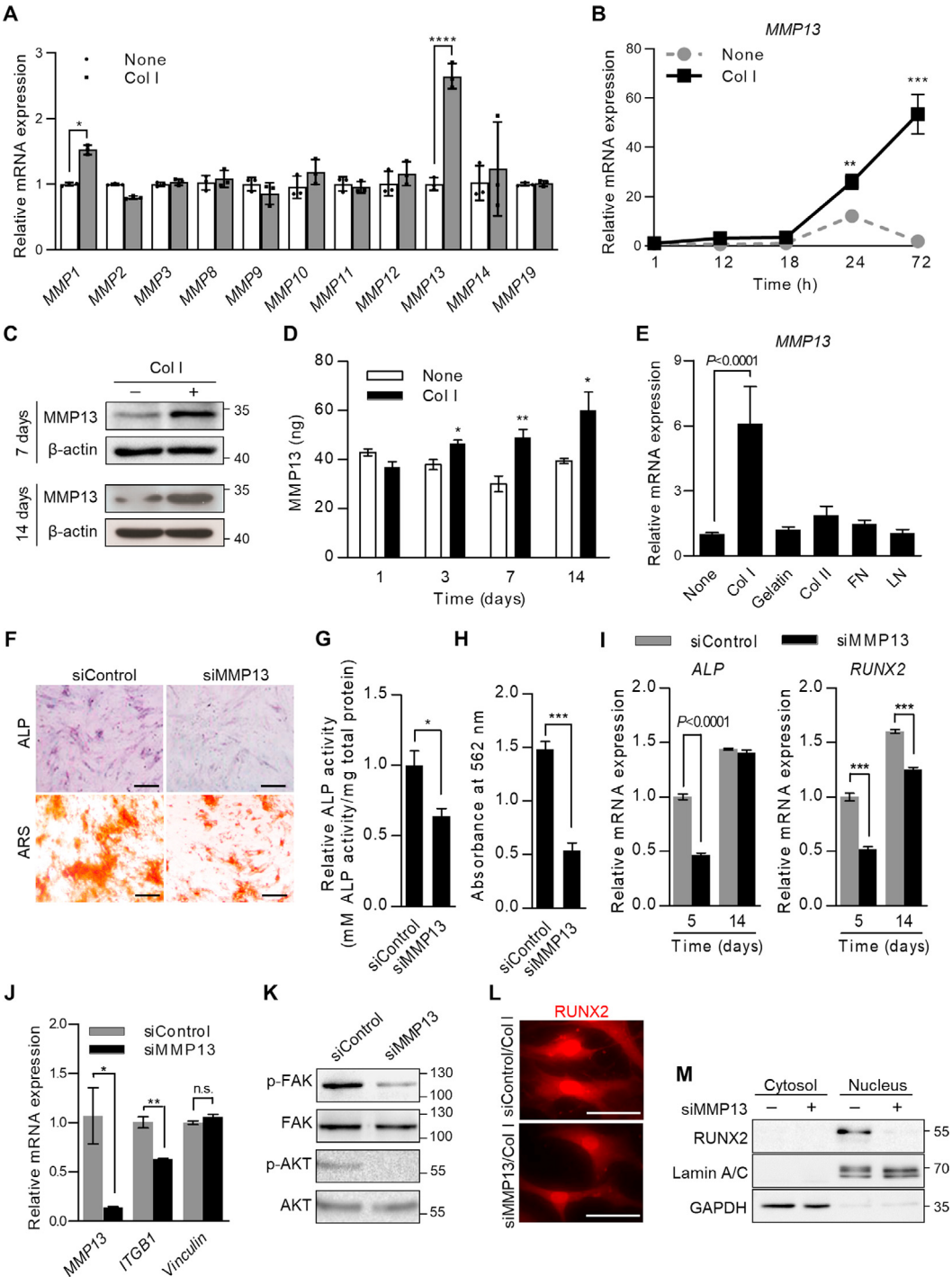

Fig. 1. Col I increases MMP13 expression during osteogenic differentiation of hMSCs. **(A)** mRNA expression of MMPs (*MMP1, MMP2, MMP3, MMP8, MMP9, MMP10, MMP11, MMP12, MMP13, MMP14,* and *MMP19*) in hMSCs after 3 days of osteogenic differentiation. The data represent the mean ± *s*.e.m. ($n = 3$) and were analyzed using two-way ANOVA and Bonferroni *post hoc* test ($^{*}P < 0.05$, $^{****}P < 0.0001$). **(B)** mRNA expression of *MMP13* in hMSCs grown on uncoated plates or a Col I matrix for up to 3 days. The data represent the mean ± *s*.e.m. ($n = 3$) and were analyzed using two-way ANOVA and Bonferroni *post hoc* test ($^{**}P < 0.01$, $^{****}P < 0.0001$). **(C)** Protein expression of intracellular MMP13 in hMSCs grown on uncoated plates or a Col I matrix for 7 and 14 days. **(D)** Secretion of MMP13 by hMSCs grown on uncoated plates or a Col I matrix for up to 14 days. Secreted MMP13 was evaluated using an MMP13-specific cleavable FRET peptide. The data represent the mean ± *s*.e.m. ($n = 4$) and were analyzed using unpaired *t*-test ($^{**}P < 0.01$). **(E)** mRNA expression of *MMP13* in hMSCs grown on uncoated plates and on Col I, gelatin, type II collagen (Col II), fibronectin (FN), and laminin (LN) matrices for 3 days. The data represent the mean ± *s*.e.m. ($n = 6$) and were analyzed using one-way ANOVA and Tukey-Kramer *post hoc* test ($^{****}P < 0.0001$, compared with None group; $^{####}P < 0.0001$, compared with Col I group). **(F)** ALP- and ARS-staining of siControl- and siMMP13-treated hMSCs grown on a Col I matrix for 5 and 14 days, respectively. Scale bars, 200 μm. **(G)** ALP activity in siControl- and siMMP13-treated hMSCs grown on a Col I matrix for 5 days. The data represent the mean ± *s*.e.m. ($n = 4$) and were analyzed using unpaired *t*-test ($^{***}P < 0.001$). **(H)** The absorbance of extracted ARS in siControl- and siMMP13-treated hMSCs grown on a Col I matrix for 5 days. The data represent the mean ± *s*.e.m. ($n = 3$) and were analyzed using unpaired *t*-test ($^{***}P<0.001$). **(I)** mRNA expression of *ALP* and *RUNX2* in siControl- and siMMP13-treated hMSCs grown on a Col I matrix for 5 and 14 days. The data represent the mean ± *s*.e.m. ($n = 3$) and were analyzed using unpaired *t*-test ($^{****}P < 0.0001$). **(J)** mRNA expression of *MMP13, ITGB1,* and *Vinculin* in siControl- and siMMP13-treated hMSCs grown on a Col I matrix for 3 days. The data represent the mean ± *s*.e.m. ($n = 3$) and were analyzed using unpaired *t*-test ($^{*}P < 0.05$, $^{**}P < 0.001$). **(K)** Protein expression of phosphorylated FAK (Y397), total FAK, phosphorylated AKT (S473), and total AKT in siControl- and siMMP13-treated hMSCs grown on a Col I matrix for 3 days. **(L)** IF analysis of RUNX2 in siControl- and siMMP13-treated hMSCs grown on a Col I matrix for 3 days. Scale bars, 50 μm. **(M)** Protein expression of RUNX2 in siControl- and siMMP13-treated hMSCs grown on a Col I matrix for 3 days.

compared with control hMSCs. In addition, hMSCs were treated with 20 ng ml^{-1} IFN-γ, IL-6, or TNF-α and grown on a Col I matrix for 24 h, and mRNA was collected 24 h after treatment to investigate the mRNA expression of MMP13 using qPCR (Fig. S4B). The resulting expression of MMP13 mRNA in IFN-γ-, IL-6-, or TNF-α-pre-treated hMSCs showed a 2.4-, 2.5-, or 4.8-fold increase, respectively.

3.3. The effect of MMP13 on osteogenic differentiation of hMSCs grown on a Col I matrix

To explore the effect of MMP13 in hMSCs grown on a Col I matrix, we knocked down *MMP13* expression using siMMP13. The knockdown of *MMP13* was confirmed by measuring MMP13 activity using an MMP13-specific cleavable peptide (Fig. S5A). First, we investigated the effect of *MMP13* knockdown on the adhesion, morphology, proliferation, and migration of hMSCs (Fig. S5B). Cell adhesion did not differ between the *MMP13*-knockdown and control hMSCs; however, proliferation increased for hMSC grown on the Col I matrix and decreased in *MMP13*-knockdown hMSCs (Fig. S5B and Fig. S2B, C). The knockdown of *MMP13* also elongated hMSCs and reduced their migration in a time-dependent manner (Fig. S5D–F). Second, we investigated the effect of knocking down *MMP13* on osteogenic differentiation. Knocking down *MMP13* decreased ALP activity, ARS staining (see Fig. 1F–H), and the mRNA expression of osteogenic markers, such as *ALP* and *RUNX2* (see Fig. 1I) in hMSCs after osteogenic differentiation. In addition, we investigated the effect of knocking down *MMP1*, as a collagenase gene, on osteogenic differentiation, which was significantly increased in the hMSCs grown on a Col I matrix (Fig. S6). The efficiency of osteogenic differentiation was determined by ALP and ARS staining (Fig. S6A). The absorbance of stained ALP (see Fig. S6B) and extracted ARS (see Fig. S6C) decreased 1.2- and 1.4-fold in the *MMP1*-knockdown hMSCs compared with the control hMSCs. These results indicate that osteogenic differentiation decreased in *MMP1*-knockdown hMSCs, which is consistent with the decrease in osteogenic differentiation seen in *MMP13*-knockdown hMSCs. Additionally, we evaluated the focal adhesion of hMSCs after binding to Col I matrix (Fig. 1J). Knocking down *MMP13* significantly decreased the expression of *ITGB1*, which is related to focal adhesion. The knockdown of *MMP13* also decreased the phosphorylation of FAK at Y397 and AKT at C473, which is related to osteogenic differentiation, but did not alter the total levels of these proteins (Fig. 1K). Knocking down *MMP13* drastically suppressed the nuclear translocation of RUNX2 in hMSCs grown on a Col I matrix (Fig. 1L, M).

3.4. rhMMP13 treatment changes the structure of Col I matrix

To investigate the structural characteristics of the MMP13-treated Col I matrix, we used rhMMP13, which was activated with 1 mM 4-aminophenylmercuric acetate and added to the Col I matrix. Subsequent SDS-PAGE revealed a single band corresponding to monomeric Col I (two α1[I] and one α2[I] chains), indicating that treatment with 50 ng ml^{-1} of activated rhMMP13 was insufficient to cleave 10 μg ml^{-1} Col I matrix (Fig. 2A). CD spectroscopy demonstrated that treatment with a relatively low concentration of activated rhMMP13 (100 ng ml^{-1}) unwound the triple-helical structure of 50 μg ml^{-1} of Col I in a time-dependent manner (Fig. 2B, C). In addition, the triple-helical structure of Col I was stained with a monoclonal antibody (green), and total Col I was stained with a polyclonal antibody (red) (Fig. 2D). After activated rhMMP13 (50 ng ml^{-1}) treatment on 50 μg ml^{-1} of Col I, the intensity of green fluorescence significantly decreased, indicating a disruption of the triple helical structure. These data were confirmed using F-CHP, which specifically binds to unwound Col I matrix (Fig. 2E). We found that F-CHP has a high binding affinity for the Col I matrix when treated with 50 ng ml^{-1} of activated rhMMP13. MMP13 is known to cleave the Col I matrix; however, the concentration of rhMMP13 (50 ng ml^{-1}; see Fig. 1D) typically secreted from hMSCs grown on a Col I matrix was too low to cleave the Col I matrix.

3.5. Growth on an rhMMP13-treated Col I matrix enhances osteogenic differentiation of hMSCs

Treatment of the Col I matrix with 10, 50, and 100 ng ml^{-1} of activated rhMMP13 (Fig. 3A) significantly increased the osteogenic capacity of hMSCs, as validated by ARS staining (Fig. 3B). The mRNA expression of the osteogenic marker genes [*RUNX2, BSP, ALP, OPN, osteonectin (ONN), COL1*, and *OSX*)] in hMSCs increased 4.0 to 18.6-fold after 14 days of osteogenic differentiation on a Col I matrix treated with 50 ng ml^{-1} of activated rhMMP13 (Fig. 3C). In addition, cell growth on an rhMMP13-treated Col I matrix increased the osteogenic differentiation of human BMMSCs (Fig. S7). We established the osteo-, adipo-, and chondrogenic differentiation of hMSCs using ALP, Oil Red O, and Alcian Blue staining 7 days after differentiation (Fig. S8), and only osteogenic differentiation was increased in hMSCs grown on an rhMMP13-treated Col I matrix. To examine the effects of other MMPs on the osteogenic differentiation of hMSCs, the cells were seeded onto a Col I matrix treated with the collagenases rhMMP1 and rhMMP8 (Fig. S9). Growth on a Col I matrix unwound by rhMMP13 as well as other collagenases (rhMMP1 and rhMMP8) facilitated the osteogenic differentiation of hMSCs; however, when high concentrations of collagenases (100 μg ml^{-1} of rhMMP8, 200 μg ml^{-1} of rhMMP8, or 200 μg ml^{-1} of rhMMP13) were added to the Col I matrix, the osteogenic differentiation of hMSCs did not increase (Fig. S9 and S10A). Indeed, *RUNX2* expression in hMSCs treated with Col I fragments did not significantly increase compared with the control (Fig. S10B). The osteogenic effect of the rhMMP13-treated Col I matrix was due to the activation of focal adhesion and the nuclear translocation of RUNX2 in hMSCs (Fig. 3D–G). In contrast, treatment with 50 ng ml^{-1} of activated rhMMP13 increased the expression of *ITGB1* and *Vinculin* (Fig. 3D). The IF images for phospho-FAK (Y397) demonstrated that treatment with activated rhMMP13 activated FAK in the siControl-treated and *MMP13*-knockdown hMSCs (Fig. 3E). As expected, rhMMP13-treated Col I matrix increased nuclear RUNX2 expression in hMSCs (see Fig. 3F, G), which directly activated the *MMP13* promoter (Fig. S10C). Together, these results indicate that a certain concentration of rhMMP13 increases the osteogenic differentiation of hMSCs by unwinding, rather than cleaving, the triple-helical structure of the Col I matrix (Fig. 3). It seems that unwinding the Col I matrix is necessary to enhance the osteogenic differentiation of MSCs.

3.6. Knocking down MMP13 decreases ITGA3 expression in hMSCs

To determine which integrin is involved in osteogenic differentiation and MMP13 expression in hMSCs grown on a Col I matrix, the mRNA expression of integrins (*ITGA1, ITGA2, ITGA3, ITGA4, ITGA5, ITGA6, ITGA10, ITGA11, ITGAV*, and *ITGB1*) was evaluated by qPCR after 3 days of osteogenic differentiation (Fig. 4A). Knocking down *MMP13* increased the expression of *ITGA4, ITGA5*, and *ITGA6* but decreased the expression of *ITGA1, ITGA3, ITGA11*, and *ITGB1* in hMSCs grown on a Col I matrix. In particular, the mRNA expression of *ITGA3* was drastically decreased (Fig. 4B). To confirm the effect of ITGA3 on the osteogenic capacity of hMSCs, we silenced the gene using siRNA (Fig. 4B). Knocking down *ITGA3* expression suppressed ALP activity compared with siControl-treated

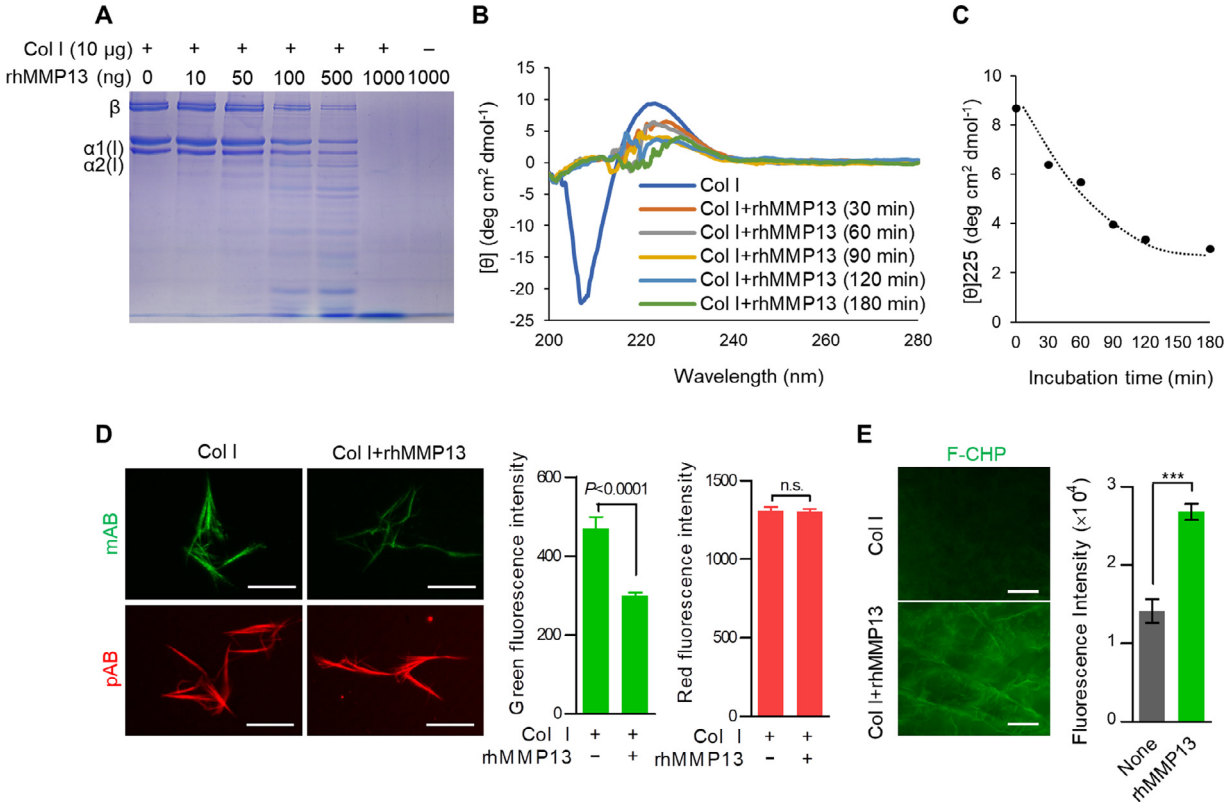

Fig. 2. MMP13 unwinds Col I. **(A)** SDS-PAGE analysis of the α1, α2, and β chains of Col I; 10 μg of Col I treated with or without rhMMP13 was loaded per lane. Chains of Col I were visualized by 0.2% Coomassie brilliant blue R-250 solution (Bio-Rad). **(B, C)** CD spectroscopy analysis of the secondary structure of Col I. Col I (50 μg) was incubated with 100 ng of rhMMP13 for 30–180 min. **(D)** Control and 50 ng ml^{-1} rhMMP13-treated Col I-coated plates were stained with monoclonal (mAB; green) and polyclonal (pAB; red) anti-Col I antibodies. Images and quantification of the fluorescence intensity (analyzed by Gen5 software, BioTek) are shown. Scale bars, 50 μm. The data represent the mean ± *s*.e.m. ($n = 8$) and were analyzed using unpaired *t*-test (****$P < 0.0001$). **(E)** Col I sponges with or without rhMMP13 were incubated with F-CHP, which binds to unwound Col I matrix. Images and quantification of the fluorescence intensity are shown. Scale bars, 200 μm. The data represent the mean ± *s*.e.m. ($n = 4$) and were analyzed using unpaired *t*-test (***$P < 0.001$).

hMSCs, and there was no difference in ALP activity between *ITGA3*-knockdown and *MMP13*-knockdown hMSCs. This indicates that ITGA3 and MMP13 are both required for the osteogenesis of hMSCs grown on a Col I matrix. Moreover, *MMP13* expression did not significantly differ between *ITGA3*-knockdown hMSCs and control hMSCs (Fig. 4C), whereas *ITGA3* expression was decreased in *MMP13*-knockdown hMSCs (Fig. 4A), which suggests that MMP13 is upstream of ITGA3 and affects its expression. In the present study, the expression of ITGA3B1 increased during the osteogenic differentiation of hMSCs grown on a Col I matrix, implying that the binding of ITGA3 to the Col I matrix is regulated by MMP13 and associated with the osteogenic differentiation of hMSCs.

3.7. Integrin binding of hMSCs grown on an rhMMP13-treated Col I matrix

In this study, we investigated the binding of ITGA3 to unwound Col I matrix. *ITGA3* expression increased in hMSCs grown on an rhMMP13-treated Col I matrix for 24 h, and the increase depended on the duration of rhMMP13 treatment (Fig. 4D). After blocking ITGA3 with a specific antibody, cell attachment was measured by imaging and quantification of the DNA content (Fig. 4E, F). Antibody-bound ITGA3 greatly decreased (0.7-fold) cell adhesion to the rhMMP13-treated Col I matrix. In addition, a direct interaction between the rhMMP13-treated Col I matrix and ITGA3 was observed using ITGA3B1-FITC (Fig. 4G). The binding affinity of ITGA3B1-FITC to the rhMMP13-treated Col I matrix was much higher than that of BSA-FITC. These findings indicate that ITGA3 plays a critical role in the adhesion of hMSCs to rhMMP13-treated Col I matrix.

3.8. rhMMP13-treated Col I sponges enhance bone tissue formation in vivo

The effect of an rhMMP13-treated Col I matrix on bone formation in vivo was determined using three types of bone defect models: a rat diaphysis defect model, a rat epiphysis defect model, and a mouse calvarial defect model. First, the Col I sponges were treated with activated rhMMP13 (1 μg of rhMMP13 per 1 mg of Col I sponge, see Fig. 5A) then implanted into the defect site ($n = 5$). In the case of the rat diaphysis defect model, *de novo* bone formation was analyzed by micro-CT and histological staining 4 weeks after implantation (Fig. 5B–D), and we found that implantation of the rhMMP13-treated Col I sponge improved bone formation with an enhanced bone volume-to-total volume (BV/TV) ratio compared to the defect group and the PBS-treated Col I sponge groups. It also reduced the total porosity (Po[*tot*]%) and increased relative bone mineral density (BMD) compared with the defect group and the PBS-treated Col I sponge groups (Fig. 5D). Histological analysis demonstrated that the rhMMP13-treated Col I sponges induced bone tissue generation in diaphysis defect regions compared with the control and non-treated Col I sponge groups (Fig. 5E). Consistent with the results of the in vivo experiment on the diaphysis defect model, bone formation in the epiphysis (see Fig. S11) and calvarial (see Fig. S12) defect regions was elevated in the rhMMP13-treated Col I sponge implant group. We theorized that the rhMMP13-treated Col I sponges induce the osteogenic differ-

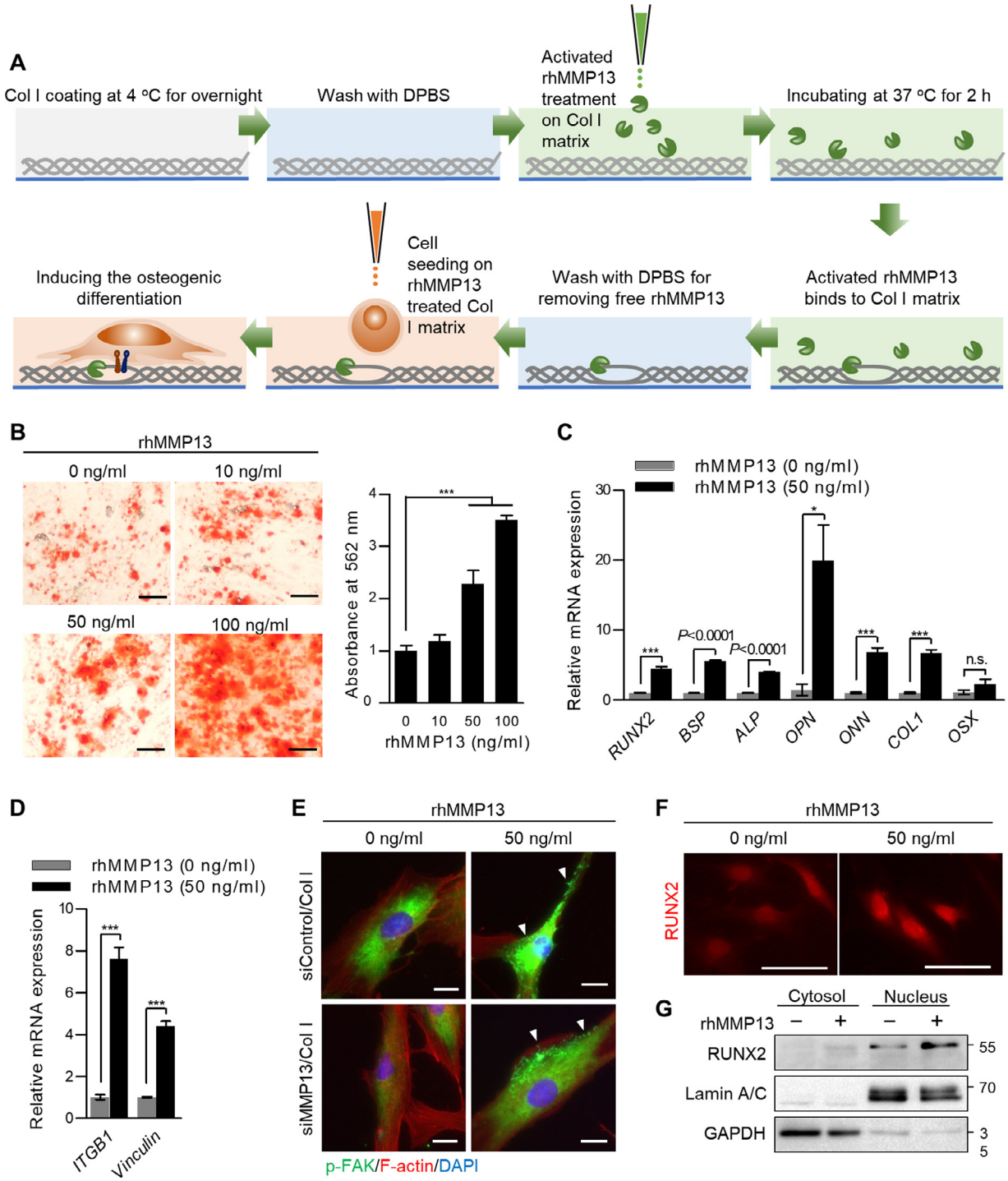

Fig. 3. Osteogenic differentiation, focal adhesion, and nuclear translocation of RUNX2 in hMSCs grown on rhMMP13-treated Col I matrix. **(A)** Representative illustration of osteogenic differentiation in hMSCs grown on an rhMMP13-treated Col I matrix. **(B)** Staining and absorbance of ARS in hMSCs grown on a Col I matrix treated with rhMMP13 for 14 days. Scale bars, 200 μm. The data represent the mean ± *s*.e.m. ($n = 4$) and were analyzed using one-way ANOVA and Tukey-Kramer *post hoc* test (***$P < 0.001$, ****$P < 0.0001$, compared with 0 ng ml^{-1} rhMMP13-treated group; ##$P < 0.01$, ####$P < 0.0001$, compared with 10 ng ml^{-1} rhMMP13-treated group; †††$P < 0.001$, compared with 50 ng ml^{-1} rhMMP13-treated group). **(C)** mRNA expression of osteogenic marker genes (*RUNX2, BSP, ALP, OPN, ONN, COL1,* and *OSX*) in rhMMP13-treated hMSCs. The data represent the mean ± *s*.e.m. ($n = 3$) and were analyzed using unpaired *t*-test (*$P < 0.05$, ***$P < 0.001$, ****$P < 0.0001$). **(D)** mRNA expression of focal adhesion-related genes (*ITGB1* and *Vinculin*) in rhMMP13-treated hMSCs. The data represent the mean ± *s*.e.m. ($n = 3$) and were analyzed using unpaired *t*-test (***$P < 0.001$). **(E)** Fluorescence staining of phosphorylated FAK (Y397) in rhMMP13-treated hMSCs grown on a Col I matrix for 3 days. Arrowheads indicate phosphorylated FAK. Scale bars, 20 μm. **(F)** Fluorescence staining of RUNX2 in rhMMP13-treated hMSCs grown on a Col I matrix for 3 days. Scale bars, 50 μm. **(G)** Comparison of the cytosolic and nuclear levels of RUNX2 in siControl- and siMMP13-treated hMSCs grown on a Col I matrix for 3 days.

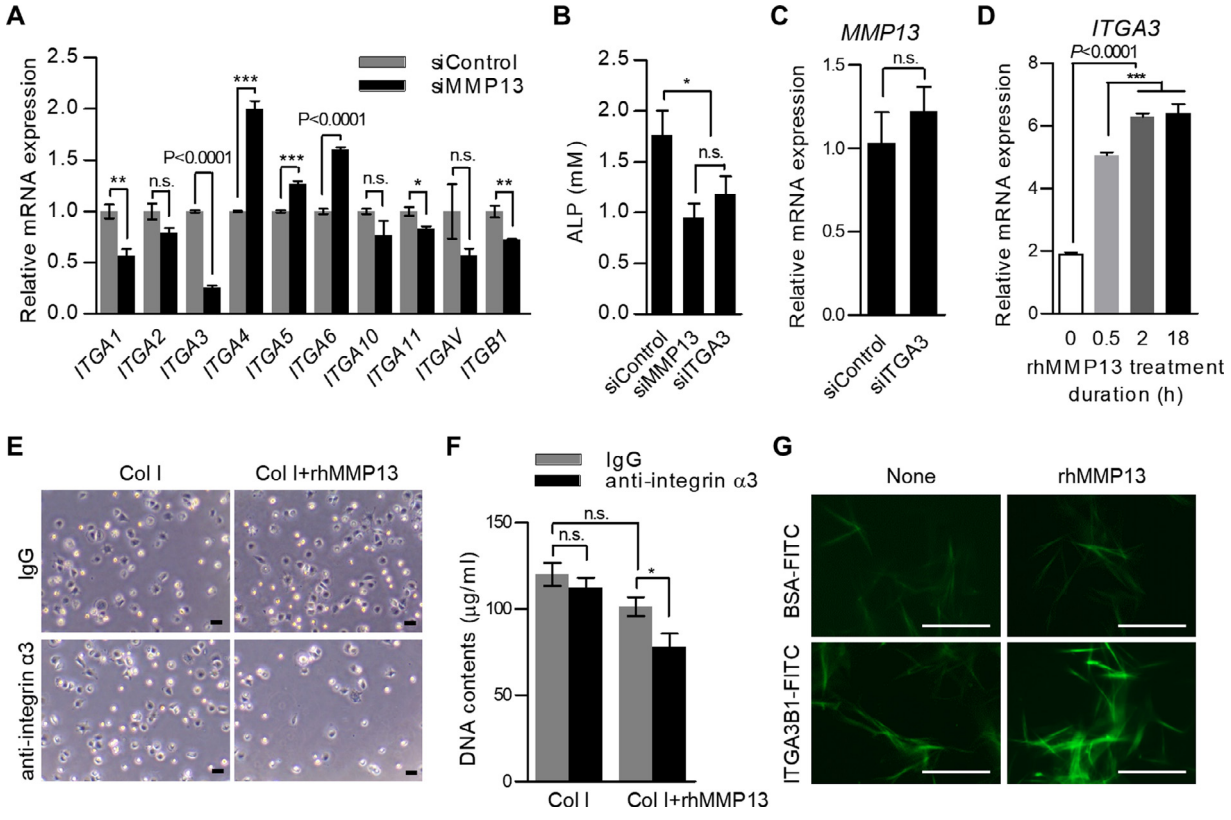

Fig. 4. Inactivating integrin $\alpha 3\beta 1$ in hMSCs reduces cell binding to rhMMP13-treated Col I matrix. **(A)** mRNA expression of integrin subunits (*ITGA1, ITGA2, ITGA3, ITGA4, ITGA5, ITGA6, ITGA10, ITGA11, ITGAV,* and *ITGB1*) in siControl- and siMMP13-treated hMSCs grown on a Col I matrix for 3 days. The data represent the mean ± *s*.e.m. ($n = 3$) and were analyzed using two-way ANOVA and Bonferroni *post hoc* test ($^{**}P < 0.01$, $^{****}P<0.0001$). **(B)** ALP activity in siControl-, siMMP13-, and siITGA3-treated hMSCs after 5 days of osteogenic differentiation. The data represent the mean ± *s*.e.m. ($n = 5$) and were analyzed using one-way ANOVA and Tukey-Kramer *post hoc* test ($^{*}P < 0.05$, $^{**}P < 0.01$, compared with siControl group). **(C)** mRNA expression of *MMP13* in siControl- and siMMP13-treated hMSCs grown on a Col I matrix for 3 days. The data represent the mean ± *s*.e.m. ($n = 3$) and were analyzed using unpaired *t*-test. **(D)** mRNA expression of *ITGA3* in hMSCs seeded on an rhMMP13-treated Col I matrix and left to adhere for 24 h. The matrix was treated with 50 ng ml^{-1} of activated rhMMP13 for 0.5, 2, or 18 h. The data represent the mean ± *s*.e.m. ($n = 3$) and were analyzed using one-way ANOVA and Tukey-Kramer *post hoc* test ($^{***}P < 0.001$, compared with 0 h treatment group; $\#\#P < 0.001$, compared with 0.5 h treatment group). **(E)** Bright-field microscopy images of hMSCs treated with IgG or an anti-integrin $\alpha 3$ antibody after being left to adhere to a non-treated or rhMMP13-treated Col I matrix for 30 min. hMSCs (10^6 cells) were pre-treated at 37 °C for 30 min with 1 μg of normal rabbit IgG (Calbiochem, cat#NI01) or anti-integrin $\alpha 3$ antibody (Abcam, cat#ab131055). The treatment concentration of activated rhMMP13 was 50 ng ml^{-1}. Scale bars, 100 μm. **(F)** Adhesion of IgG- or anti-integrin $\alpha 3$ antibody-treated hMSCs to a non-treated or rhMMP13-treated Col I matrix after being left to adhere for 30 min was quantified by measuring the DNA content (Quant-iT PicoGreen dsDNA Assay Kit; Invitrogen). The treatment concentration of activated rhMMP13 was 50 ng ml^{-1}. The data represent the mean ± *s*.e.m. ($n = 6$) and were analyzed using two-way ANOVA and Bonferroni *post hoc* test ($^{**}P < 0.01$, IgG-treated MSCs grown on a Col I matrix vs. anti-integrin $\alpha 3$ antibody-treated MSCs grown on an rhMMP13-treated Col I matrix; $\#\#P < 0.01$, anti-integrin $\alpha 3$ antibody-treated MSCs grown on a Col I matrix vs. anti-integrin $\alpha 3$ antibody-treated MSCs grown on an rhMMP13-treated Col I matrix). **(G)** Fluorescence images of BSA-FITC and ITGA3B1-FITC on a Col I matrix treated with 50 ng ml^{-1} of rhMMP13. Scale bars, 50 μm.

entiation of hMSCs recruited to the long bone (diaphysis and epiphysis) and calvarial defects (Fig. 5F).

4. Discussion

In this study, we screened various members of the MMP family. Reportedly, MMPs are important for bone development during embryogenesis, and the expression of MMP13, but not MMP2 or MMP9, was significantly increased during the osteogenic differentiation of hMSCs grown on a Col I matrix (Fig. 1A). These MMP family members have catalytic properties that lead to the cleavage of the Col I peptide, and the binding and unwinding of the triple helical structure of Col I matrix is caused by collagenases, including MMP13 [38]. When the bones were fractured, we found that COL1 and MMP13 were expressed at the defect lesions (Fig. S1), and we suggested that Col I matrix would be remodeled by MMP13 during bone regeneration in vivo. Indeed, treatment with activated rhMMP13 at a range of concentrations (up to 50 ng of rhMMP13 per 10 μg of Col I matrix) unwound, but did not cleave, the triple-helical structure of the Col I matrix (Fig. 2). At the optimum concentration of 50 ng ml^{-1}, rhMMP13 increased the osteogenic differentiation of hMSCs by unwinding the triple-helical structure of the Col I matrix (Fig. 3). Apparently, the unwinding of the Col I matrix is necessary to enhance the osteogenic differentiation of MSCs. MMP1 and MMP8 as a collagenase are also able to promote osteogenic differentiation of MSCs through the same mechanism as that of MMP13 presumably because the Col I matrix can be unwound by collagenases (Fig. S9). However, the expression of MMP13 was significantly increased compared to other types of MMPs in MSCs grown on a Col1 matrix (Fig. 1A). Based on this result, we tried to focus on MMP13 rather than others and hypothesized that MSCs, which contribute to a self-healing of bone, promote bone regeneration following the unwinding of Col I matrix by up-regulation of MMP13. Besides, several previous studies have supported that MMP13 plays an important role in bone regeneration or development [18–21].

Recently, heat-denatured collagen was reported to enhance the osteogenic differentiation of MSCs and the differentiation of pre-osteoblasts via interaction with an exposed cryptic arginine-glycine-aspartic acid (RGD) sequence [39,40]. Consistent with this, another study reported that proteolytic enzymes can expose a cryptic RGD sequence in the ECM [41]. However, neither study

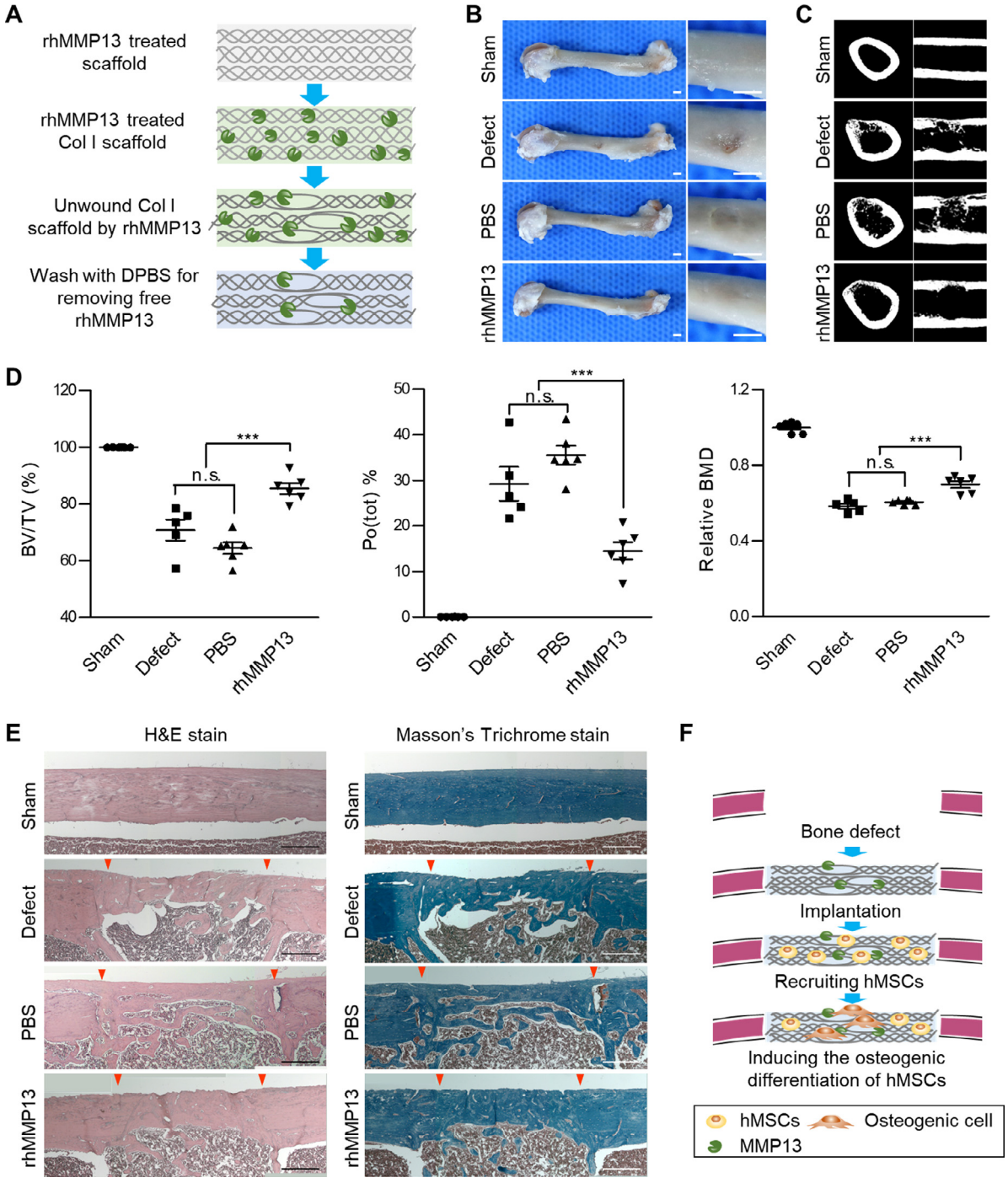

Fig. 5. Bone formation upon transplantation of rhMMP13-treated Col I sponges. **(A)** Graphic illustration of rhMMP13-treated Col I sponge. **(B)** Gross images of the long bone of a control rat with a defect 4 weeks after implantation of a DPBS-treated Col I sponge or an rhMMP13-treated Col I sponge (1 μg of rhMMP13 per 1 mg of sponge). Scale bars, 2 mm. **(C)** Micro-CT images and **(D)** quantitative micro-CT data. The bone volume per tissue volume (BV/TV), total porosity (Po[*tot*]), and relative bone mineral density (BMD) of the sham-operated model (control) were normalized to 100%, 0%, and 1, respectively. The data represent the mean ± *s*.e.m. ($n = 5$) and were analyzed using one-way ANOVA and Tukey-Kramer *post hoc* test (***$P < 0.001$, ****P 0.0001, compared with Sham group; ###$P < 0.001$, compared with Defect group; †††$P < 0.001$, ††††$P <$ 0.0001, compared with PBS group). **(E)** Histological images of hematoxylin, eosin, and Masson's trichrome staining. Arrows indicate the defect margins. Scale bars, 500 μm. **(F)** Graphic illustration of bone healing after implantation of rhMMP13-treated Col I sponge.

mentioned MMPs or clearly explained how ECM remodeling is involved in integrin binding. A few research groups have reported that ITGA3B1 binds to the RGD sequence [42,43]. We found that expression of ITGA3 increased in hMSCs grown on an rhMMP13-treated Col I matrix but decreased in *MMP13*-knockdown hMSCs, even in cells grown on a Col I matrix (Fig. 4A, D). However, MMP13 expression did not decrease in the *ITGA3*-knockdown hMSCs, suggesting that MMP13 is upstream of ITGA3 and affects its expression, which implies that the binding of ITGA3 to the Col I matrix is regulated by MMP13 and associated with the osteogenic differentiation of hMSCs.

Inflammation is the first response in the repair of bone fractures and is associated with pro-inflammatory cytokines such as IL-1β and TNF-α. MMPs are included in the inflammatory pro-

cesses, and IL-1β and TNF-α are known to induce MMP3 and MMP13 expression in chondrocytes [44]. When hMSCs were grown on uncoated plates, we found that the secretion of MMP13 increased in inflammatory conditions (Fig. S4). Based on this result, we suggest that the secretion of MMP13 may be induced by pro-inflammatory cytokines secreted at the bone defect lesion and MMP13 is involved in bone healing through remodeling of the Col I matrix.

Integrin is known to initiate the intracellular signal cascades related to osteogenic differentiation by inducing the phosphorylation of FAK and subsequently activating AKT to regulate the stability and transcriptional efficiency of RUNX2, the main transcription factor for osteogenic differentiation [45]. When integrin is activated through the binding of a specific ligand, it causes the recruitment of the focal adhesion complex, including FAK and vinculin, according to stimulation by sub-signaling transduction. Consequently, phosphorylated RUNX2 stimulates the activation of the *MMP13* promoter [46,47]. In this study, knocking down *MMP13* decreased the expression of RUNX2 and the phosphorylation of FAK and AKT (Fig. 1K-M). Although *MMP13* knockdown did not induce a decrease in vinculin expression by hMSCs, it seems that the focal adhesion signaling cascade decreased because of the downregulation of phosphorylated FAK and ITGB1, which can be dimerized with integrin α3. To stimulate the signaling cascade, the activation of signaling molecules, such as by phosphorylation, is more important than their expression at the mRNA or protein level. However, RUNX2 can directly activate the *MMP13* promoter (Fig. S10C), indicating that the signaling cascade initiated by phosphorylation of FAK and AKT is responsible for activating *MMP13* expression by RUNX2.

Although our findings cannot fully demonstrate the mechanisms underlying the self-healing of bone tissue in the body, they will be a valuable knowledge base for researchers elucidating the fundamental mechanisms of self-healing and developing efficient therapeutics for bone tissue regeneration. In addition, we hope the results of this study will contribute to improving patient quality of life and the advancement of scientific technology through further research into the development and application of biomaterials with enhanced bone tissue regeneration efficiency.

5. Conclusion

In conclusion, we found that exposing the cryptic ligand on Col I matrix to MMP13 activates integrins, especially integrin $\alpha3\beta1$, which stimulates a signaling cascade through focal adhesion molecules (Fig. S13). This signaling pathway triggers the translocation of RUNX2 into the nucleus, where it binds to the *MMP13* promoter and upregulates expression of the gene. We propose that an MMP13/ITGA3/RUNX2 positive feedback loop operates in stem cells grown on a Col I matrix; this could explain how bone fractures undergo self-healing. Furthermore, an MMP13-treated Col I matrix can be used to specifically promote the osteogenic differentiation of hMSCs and bone tissue self-healing.

Declaration of Competing Interest

The authors declare that they have no known competing financial interests or personal relationships that could have appeared to influence the work reported in this paper.

Acknowledgments

This work was funded by the Korean government (MSIT and MOE) (NRF-2019R1A2B5B03069690, NRF-2019M3A9H1032376, NRF-2020R1I1A1A01074331, and NRF-2020H1D3A1A02078382) and supported by the Dongguk University Research Fund of 2018.

Supplementary materials

Supplementary material associated with this article can be found, in the online version, at doi:10.1016/j.actbio.2021.02.042.

References

[1] T.A. Einhorn, L.C. Gerstenfeld, Fracture healing: mechanisms and interventions, Nat. Rev. Rheumatol. 11 (1) (2015) 45–54.
[2] B. Corradetti, M.G. Marini, C.P. Lentini, I. Giretti, D. Bizzaro, Resident Stem Cells Stimulation: New Promise For Tissue Regeneration?, OMICS Group, 2015 eBooks.
[3] R.C. Rennert, M. Sorkin, R.K. Garg, G.C. Gurtner, Stem cell recruitment after injury: lessons for regenerative medicine, Regen. Med. 7 (6) (2012) 833–850.
[4] M.S. Rahman, N. Akhtar, H.M. Jamil, R.S. Banik, S.M. Asaduzzaman, TGF–beta/BMP signaling and other molecular events: regulation of osteoblastogenesis and bone formation, Bone Res. 3 (2015) 15005.
[5] Y. Bi, D. Ehirchiou, T.M. Kilts, C.A. Inkson, M.C. Embree, W. Sonoyama, L. Li, A.I. Leet, B.M. Seo, L. Zhang, S. Shi, M.F. Young, Identification of tendon stem/progenitor cells and the role of the extracellular matrix in their niche, Nat. Med. 13 (10) (2007) 1219–1227.
[6] P.G. Robey, N.S. Fedarko, T.E. Hefferan, P. Bianco, U.K. Vetter, W. Grzesik, A. Friedenstein, G. Van der Pluijm, K.P. Mintz, M.F. Young, J.M. Kerr, K. Ibaraki, A.M. Heegaard, Structure and molecular regulation of bone matrix proteins, Journal of bone and mineral research: the official journal of the American Society for Bone and Mineral Research 8 (Suppl 2) (1993) S483–S487.
[7] C. Gentili, R. Cancedda, Cartilage and bone extracellular matrix, Curr. Pharm. Des. 15 (12) (2009) 1334–1348.
[8] S.W. Lane, D.A. Williams, F.M. Watt, Modulating the stem cell niche for tissue regeneration, Nat. Biotechnol. 32 (8) (2014) 795–803.
[9] P. Lu, K. Takai, V.M. Weaver, Z. Werb, Extracellular matrix degradation and remodeling in development and disease, Cold Spring Harb. Perspect Biol. 3 (12) (2011).
[10] K.S. Tsai, S.Y. Kao, C.Y. Wang, Y.J. Wang, J.P. Wang, S.C. Hung, Type I collagen promotes proliferation and osteogenesis of human mesenchymal stem cells via activation of ERK and Akt pathways, J. Biomed. Mater. Res. A 94 (3) (2010) 673–682.
[11] T. Gong, J. Xie, J. Liao, T. Zhang, S. Lin, Y. Lin, Nanomaterials and bone regeneration, Bone Res. 3 (2015) 15029.
[12] J. Henkel, M.A. Woodruff, D.R. Epari, R. Steck, V. Glatt, I.C. Dickinson, P.F. Choong, M.A. Schuetz, D.W. Hutmacher, Bone Regeneration Based on Tissue Engineering Conceptions - A 21st Century Perspective, Bone Res. 1 (3) (2013) 216–248.
[13] A. Bernhardt, A. Lode, S. Boxberger, W. Pompe, M. Gelinsky, Mineralised collagen–an artificial, extracellular bone matrix–improves osteogenic differentiation of bone marrow stromal cells, J. Mater. Sci. Mater. Med. 19 (1) (2008) 269–275.
[14] S.P. Bruder, D.J. Fink, A.I. Caplan, Mesenchymal stem cells in bone development, bone repair, and skeletal regeneration therapy, J. Cell. Biochem. 56 (3) (1994) 283–294.
[15] D.J. Behonick, Z. Xing, S. Lieu, J.M. Buckley, J.C. Lotz, R.S. Marcucio, Z. Werb, T. Miclau, C. Colnot, Role of matrix metalloproteinase 13 in both endochondral and intramembranous ossification during skeletal regeneration, PLoS ONE 2 (11) (2007) e1150.
[16] K.B. Paiva, J.M. Granjeiro, Bone tissue remodeling and development: focus on matrix metalloproteinase functions, Arch. Biochem. Biophys. 561 (2014) 74–87.
[17] J.M. Howes, D. Bihan, D.A. Slatter, S.W. Hamaia, L.C. Packman, V. Knauper, R. Visse, R.W. Farndale, The recognition of collagen and triple-helical toolkit peptides by MMP-13: sequence specificity for binding and cleavage, J. Biol. Chem. 289 (35) (2014) 24091–24101.
[18] V. Mattot, M.B. Raes, P. Henriet, Y. Eeckhout, D. Stehelin, B. Vandenbunder, X. Desbiens, Expression of interstitial collagenase is restricted to skeletal tissue during mouse embryogenesis, J. Cell. Sci. 108 (Pt 2) (1995) 529–535.
[19] X. Wang, P.A. Manner, A. Horner, L. Shum, R.S. Tuan, G.H. Nuckolls, Regulation of MMP-13 expression by RUNX2 and FGF2 in osteoarthritic cartilage, Osteoarthritis and cartilage /OARS, Osteoarthritis Research Society 12 (12) (2004) 963–973.
[20] Q. Wu, K. Wang, X. Wang, G. Liang, J. Li, Delivering siRNA to control osteogenic differentiation and real-time detection of cell differentiation in human mesenchymal stem cells using multifunctional gold nanoparticles, J. Mater. Chem. B 8 (15) (2020) 3016–3027.
[21] K. Wang, Q. Wu, X. Wang, G. Liang, A. Yang, J. Li, Near-infrared control and real-time detection of osteogenic differentiation in mesenchymal stem cells by multifunctional upconversion nanoparticles, Nanoscale 12 (18) (2020) 10106–10116.
[22] S. Barthelemi, J. Robinet, R. Garnotel, F. Antonicelli, E. Schittly, W. Hornebeck, S. Lorimier, Mechanical forces-induced human osteoblasts differentiation involves MMP-2/MMP-13/MT1-MMP proteolytic cascade, J. Cell. Biochem. 113 (3) (2012) 760–772.
[23] S.Y. Tang, R.P. Herber, S.P. Ho, T. Alliston, Matrix metalloproteinase-13 is required for osteocytic perilacunar remodeling and maintains bone fracture resistance, Journal of bone and mineral research: the official journal of the, Am. Soc. Bone Mineral Res. 27 (9) (2012) 1936–1950.

[24] N. Kosaki, H. Takaishi, S. Kamekura, T. Kimura, Y. Okada, L. Minqi, N. Amizuka, U.I. Chung, K. Nakamura, H. Kawaguchi, Y. Toyama, J. D'Armiento, Impaired bone fracture healing in matrix metalloproteinase-13 deficient mice, Biochem. Biophys. Res. Commun. 354 (4) (2007) 846–851.
[25] J. Yue, K. Zhang, J. Chen, Role of integrins in regulating proteases to mediate extracellular matrix remodeling, Cancer Microenviron. 5 (3) (2012) 275–283.
[26] C. Zaragoza, E. Lopez-Rivera, C. Garcia-Rama, M. Saura, A. Martinez-Ruiz, T.R. Lizarbe, F. Martin-de-Lara, S. Lamas, Cbfa-1 mediates nitric oxide regulation of MMP-13 in osteoblasts, J. Cell. Sci. 119 (Pt 9) (2006) 1896–1902.
[27] C. Bonnans, J. Chou, Z. Werb, Remodelling the extracellular matrix in development and disease, Nat. Rev. Mol. Cell Biol. 15 (12) (2014) 786–801.
[28] W.P. Daley, S.B. Peters, M. Larsen, Extracellular matrix dynamics in development and regenerative medicine, J. Cell. Sci. 121 (Pt 3) (2008) 255–264.
[29] Z. Hamidouche, O. Fromigue, J. Ringe, T. Haupl, P. Vaudin, J.C. Pages, S. Srouji, E. Livne, P.J. Marie, Priming integrin alpha5 promotes human mesenchymal stromal cell osteoblast differentiation and osteogenesis, Proc. Natl. Acad. Sci. U.S.A. 106 (44) (2009) 18587–18591.
[30] M. Witkowska-Zimny, E. Wrobel, Mrowka, alpha2beta1 integrin-mediated mechanical signals during osteodifferentiation of stem cells from the Wharton's jelly of the umbilical cord, Folia Histochem. Cytobiol. 52 (4) (2014) 297–307.
[31] R.F. Klees, R.M. Salasznyk, K. Kingsley, W.A. Williams, A. Boskey, G.E. Plopper, Laminin-5 induces osteogenic gene expression in human mesenchymal stem cells through an ERK-dependent pathway, Mol. Biol. Cell. 16 (2) (2005) 881–890.
[32] C. Popov, T. Radic, F. Haasters, W.C. Prall, A. Aszodi, D. Gullberg, M. Schieker, D. Docheva, Integrins [alpha]2[*beta*]1 and [alpha]11[*beta*]1 regulate the survival of mesenchymal stem cells on collagen I, Cell. Death Dis. 2 (2011) e186.
[33] Z. Saidak, C.Le Henaff, S. Azzi, C. Marty, S. Da Nascimento, P. Sonnet, P.J. Marie, Wnt/β-Catenin Signaling Mediates Osteoblast Differentiation Triggered by Peptide-induced $\alpha 5\beta 1$ Integrin Priming in Mesenchymal Skeletal Cells, J. Biol. Chem. 290 (11) (2015) 6903–6912.
[34] A. Di Benedetto, G. Brunetti, F. Posa, A. Ballini, F.R. Grassi, G. Colaianni, S. Colucci, E. Rossi, E.A. Cavalcanti-Adam, L. Lo Muzio, M. Grano, G. Mori, Osteogenic differentiation of mesenchymal stem cells from dental bud: role of integrins and cadherins, Stem. Cell Res. 15 (3) (2015) 618–628.
[35] J. Jokinen, E. Dadu, P. Nykvist, J. Kapyla, D.J. White, J. Ivaska, P. Vehvilainen, H. Reunanen, H. Larjava, L. Hakkinen, J. Heino, Integrin-mediated cell adhesion to type I collagen fibrils, J. Biol. Chem. 279 (30) (2004) 31956–31963.
[36] D. Gullberg, K.R. Gehlsen, D.C. Turner, K. Ahlen, L.S. Zijenah, M.J. Barnes, K. Rubin, Analysis of alpha 1 beta 1, alpha 2 beta 1 and alpha 3 beta 1 integrins in cell–collagen interactions: identification of conformation dependent alpha 1 beta 1 binding sites in collagen type I, Embo. J. 11 (11) (1992) 3865–3873.
[37] Y. Tang, R.G. Rowe, E.L. Botvinick, A. Kurup, A.J. Putnam, M. Seiki, V.M. Weaver, E.T. Keller, S. Goldstein, J. Dai, D. Begun, T. Saunders, S.J. Weiss, MT1-MMP-dependent control of skeletal stem cell commitment via a beta1-integrin/YAP/TAZ signaling axis, Dev. Cell 25 (4) (2013) 402–416.
[38] A.J. Messent, D.S. Tuckwell, V. Knauper, M.J. Humphries, G. Murphy, J. Gavrilovic, Effects of collagenase-cleavage of type I collagen on alpha2beta1 integrin-mediated cell adhesion, J. Cell Sci. 111 (8) (1998) 1127–1135.
[39] J.R. Mauney, C. Kirker-Head, L. Abrahamson, G. Gronowicz, V. Volloch, D.L. Kaplan, Matrix-mediated retention of in vitro osteogenic differentiation potential and in vivo bone-forming capacity by human adult bone marrow-derived mesenchymal stem cells during ex vivo expansion, J. Biomed. Mater. Res. A 79 (3) (2006) 464–475.
[40] A.V. Taubenberger, M.A. Woodruff, H. Bai, D.J. Muller, D.W. Hutmacher, The effect of unlocking RGD-motifs in collagen I on pre-osteoblast adhesion and differentiation, Biomaterials 31 (10) (2010) 2827–2835.
[41] J. Heino, The collagen family members as cell adhesion proteins, Bioessays 29 (10) (2007) 1001–1010.
[42] E. Ruoslahti, RGD and other recognition sequences for integrins, Annu. Rev. Cell Dev. Biol. 12 (1996) 697–715.
[43] R. Pankov, K.M. Yamada, Fibronectin at a glance, J. Cell Sci. 115 (Pt 20) (2002) 3861–3863.
[44] A. Liacini, J. Sylvester, W.Q. Li, M. Zafarullah, Mithramycin downregulates proinflammatory cytokine-induced matrix metalloproteinase gene expression in articular chondrocytes, Arthritis Res. Ther. 7 (4) (2005) R777–R783.
[45] J.L. Fowlkes, R.C. Bunn, K.M. Thrailkill, Contributions of the Insulin/Insulin-Like Growth Factor-1 Axis to Diabetic Osteopathy, J. Diabetes Metab. 1 (3) (2011).
[46] N. Selvamurugan, E. Shimizu, M. Lee, T. Liu, H. Li, N.C. Partridge, Identification and characterization of Runx2 phosphorylation sites involved in matrix metalloproteinase-13 promoter activation, FEBS Lett. 583 (7) (2009) 1141–1146.
[47] E. Shimizu, T. Nakatani, Z. He, N.C. Partridge, Parathyroid hormone regulates histone deacetylase (HDAC) 4 through protein kinase A-mediated phosphorylation and dephosphorylation in osteoblastic cells, J. Biol. Chem. 289 (31) (2014) 21340–21350.